Long-Term Quantitative Analysis of Inner Retinal Dimples and Visual Function Post Internal Limiting Membrane Peeling in Macular Diseases

Yubo Wu · Yiqi Chen · Jianbo Mao · Xin Ye · Huan Chen ·
Zhaokai Xu · Lijun Shen

ABSTRACT

Introduction: Inner retinal dimples (IRDs) are frequently detected after internal limiting membrane (ILM) peeling. However, the distribution of IRDs and its effect on postoperative visual function remain unclear. We aim to quantify the distribution of IRDs after ILM peeling in different macular diseases and analyze its influence on postoperative visual function.

Methods: We retrospectively reviewed patients undergoing vitrectomy with ILM peeling and followed up until 12 months in our center. The distribution of IRDs were quantitatively determined using optical coherence tomography (OCT) and OCT angiography in a different sector of Early Treatment Diabetic Retinopathy Study grid. Visual function was evaluated by retinal sensitivity (RS) using microperimetry. Spearman correlation was performed between RS and IRDs within the same sectors.

Multivariate linear regression analysis was performed to analyze the association between baseline characteristics and IRDs.

Results: A total of 43 idiopathic macular hole (iMH) cases, 56 idiopathic epiretinal membrane (iERM) cases and 42 myopic foveoschisis (mFS) cases were included. IRDs increased gradually at ILM-peeled area, interrupting ganglion cell layer. Most IRDs were observed in temporal sector. A negative correlation was depicted between the increase of IRDs and the progress of RS at both perifovea and parafovea in iERM, but only at perifovea in iMH. No significant correlation between the change of IRDs and RS was found in mFS. Multivariable linear regression model showed that preoperative axial length was significantly associated with postoperative IRDs in all patients.

Conclusions: IRDs distributed mostly at temporal sector after ILM peeling, interrupting ganglion cell layer. IRD progression may influence postoperative RS only in iMH and iERM. Ophthalmologists may avoid temporal sector especially in eyes with normal axial length or strong ILM–ERM adherence.

Keywords: Internal limiting membrane; Inner retinal dimples; Temporal; Retinal sensitivity

Y. Wu · Z. Xu · L. Shen (✉)
National Clinical Research Center for Ocular Diseases, Eye Hospital, Wenzhou Medical University, 270 Xueyuan West Road, Wenzhou 325027, Zhejiang Province, China
e-mail: slj@mail.eye.ac.cn

Present Address:
Y. Chen · J. Mao · X. Ye · H. Chen · L. Shen
Department of Ophthalmology, Zhejiang Provincial People's Hospital (Affiliated People's Hospital, Hangzhou Medical College), Hangzhou, China

Key Summary Points

Why carry out this study?

Internal limiting membrane (ILM) peeling is a widely acknowledged procedure in the treatment for traction maculopathies. Inner retinal dimples (IRDs) are often detected postoperatively. However, the distribution of IRDs and its effect on visual function remain unknown.

In this study, we explore the natural course and distribution of IRDs after ILM peeling and hypothesize that IRDs may influence visual function.

What was learned from this study?

IRDs were distributed mostly at the temporal sector of the ILM peeled area after surgery. Ophthalmologists may avoid temporal sector of fovea during ILM peeling.

The progression of IRDs may influence postoperative retinal sensitivity (RS) in idiopathic macular hole (iMH) and idiopathic epiretinal membrane (iERM).

INTRODUCTION

Internal limiting membrane (ILM) peeling provides promising therapeutic outcomes in macular disease, such as increasing the closure rate of idiopathic macular hole (iMH), reducing the recurrence of idiopathic epiretinal membrane (iERM), assisting foveal reattachment in myopic foveoschisis (mFS). However, the effect of ILM peeling on visual function remains controversial [1]. ILM peeling has been reported to be associated with the decrease of macular thickness [2] and the recovery postponement of b-wave amplitudes in focal macular electroretinograms [3]. In 2001, Tadayoni et al. [4] first found inner retinal dimples (IRDs) on a B-scan of optical coherence tomography (OCT)

after epiretinal membrane removal, which coincided with the dark arcuate striae along the course of the optic nerve fibers on a C-scan of OCT, which was the so called "dissociated optic nerve fiber layer (DONFL)." Since then, IRDs (or DONFL) have been reported to appear after ILM peeling in various diseases [5–7]. Some studies [8–10] pointed out that IRDs might contribute to the decrease of visual function after ILM peeling. Others [11–13] insisted no difference in retinal sensitivity (RS) between arcuate striae and normal retina. However, the majority of previous studies only depicted IRDs in iMH, overlooking other macular diseases such as iERM and mFS. Additionally, the measure equipment or method in the above-mentioned studies may have failed to detect a mild degree of inner retinal defect in whole ILM peeling area. Using the newest Nidek's microperimetry (MP-3), we previously confirmed high incidence of scotomas in iMH patients with IRDs [7]. Nevertheless, the natural course of IRDs after ILM peeling and its impact on visual function in other macular diseases remain uncertain.

In the present study, we evaluated IRDs and RS in different sectors using optical coherence tomography angiography (OCTA), spectral-domain optical coherence tomography (SD–OCT), and MP-3 at multiple postoperative timepoints in patients with iMH, iERM, or mFS undergoing pars plana vitrectomy (PPV) combined with ILM peeling. We aimed to investigate the pattern of postoperative IRDs and its impact on visual function.

METHODS

Ethical Approval

Procedures using medical records were conducted in accordance with the tenets of the Declaration of Helsinki and were approved by the Affiliated Eye Hospital of Wenzhou Medical University, Hangzhou, China (Ethics approval ID: H2022-014-K-14). All participants or their legal representatives signed the informed consent that their information including demographic and examination data may be used for scientific research.

Subjects

This retrospective study screened the data of 118 iERM cases, 76 iMH cases, and 66 mFS cases of patients who underwent PPV at the Affiliated Eye Hospital of Wenzhou Medical University between January 2019 and December 2022. The inclusion criteria were: (1) ILM peeling was performed during PPV, and (2) high-quality images of the postoperative macular conditions were obtained at 1, 3, 6, or 12 months (1 M, 3 M, 6 M, 12 M) after surgery. The exclusion criteria were as follows: (1) any kind of systemic diseases, (2) history of ocular trauma or ocular surgery, (3) any other retinopathy or choroidopathy, and (4) lost to more than three follow-ups of the four timepoints (1 M, 3 M, 6 M, and 12 M).

Surgical Procedure

All surgeries were performed by the same experienced surgeon (Lijun Shen). The surgical procedure consisted of a 23-gauge PPV with induced posterior vitreous detachment. After removing vitreous and checking peripheral retina thoroughly, 0.3 ml 0.025% indocyanine green (ICG) was injected into the vitreous cavity to stain the ILM for 30 s. After rinsing excess ICG, ILM was pinched at 1 optic disk (PD) away from the foveola, either superiorly or inferiorly, and peeled in a circular manner with retinal forceps. The peeled area covered approximately 3 PD in diameter. Finally, complete air–fluid exchange was performed using sterilized air. Perfluoropropane (C3F8) or silicone oil as a tamponade might be used in the discretion of the surgeon, depending on the duration of disease and retina structure on OCT image. Cataract surgery was performed in the phakic eyes if necessary.

Ophthalmological Examination

Baseline ophthalmological examinations included slit-lamp examination, intraocular pressure measurement by noncontact tonometry, best-corrected visual acuity (BCVA) by comprehensive optometry, axial length by optical biometer (Carl Zeiss Meditec), OCT (Spectralis; Heidelberg Engineering, Heidelberg, Germany), optical coherence tomography angiography (OCTA) (AngioVue; Optovue, Inc., Fremont, CA, USA), and MP-3 (NIDEK, Gamagori, Japan). Follow-up ophthalmological examinations included slit-lamp examination, intraocular pressure, BCVA, OCT, and MP-3. After the baseline visit, all postoperative examinations were performed using the "follow-up" mode.

The BCVA was recorded in decimal acuity and then converted to logarithm of the minimal angle of resolution (logMAR) value for statistical analyses. To quantify visual acuity in eyes with low vision, counting fingers' visual acuity was assigned the logMAR units of 1.7, 1.85, 1.90, and 2.00, based on the different distances of measurement and hand motion visual acuity of 2.30 [12].

OCT and OCTA Image Acquisition and Data Analysis

To determine the quantity and distribution of IRDs and to explore the relationship between dynamic changes of IRDs with macular sensitivity, we used the Early Treatment Diabetic Retinopathy Study (ETDRS) grid to assure that en-face OCT, OCTA, and MP-3 can analyze within the same sector at each timepoint of follow-up. According to the ETDRS grid, the central $6 \times 6 \, mm^2$ macular area was separated as the parafovea ring and the perifovea ring, each ring was divided into four sectors for further analysis. The parafovea ring included inner superior (S1), inner inferior (I1), inner nasal (N1), and inner temporal (T1). The perifovea ring included outer superior (S2), outer inferior (I2), outer nasal (N2), and outer temporal (T2) (Fig. 1). Based on the built-in software (Angio-Vue version 2017.1.0.155 software), the vessel density (VD) of the superficial capillary plexus (SCP) of OCTA images in each sector were segmented and generated automatically, noted as superficial vessel density (SVD) (Fig. 1A). The boundary of SCP was set from ILM to 9 μm below the inner plexiform layer (IPL).

To semiquantitatively evaluate the severity of IRDS, the $6 \times 6 \, mm^2$ area was further divided

into 20 × 20 squares of the same size [14]. The number of the grids containing IRDs was counted manually in each ETDRS subfield (Fig. 1B, Fig. 2). The depth of IRDs was clarified by cross-sectional OCT images of macular foveal pit.

MP-3 Image Acquisition and Data Analysis

RS values were obtained by the 4–2–1 staircase strategy with a Goldmann III size stimulus. The total of 61 stimulus points covered 20 degrees of visual field. A customized method of two concentric circles was used to delimit 10 degrees and 20 degrees diameter to set up correspondence with parafovea and perifovea, respectively [7, 15]. Thus, 28 points were defined in a 10-degree area (1 point at foveal center was excluded on account of avoiding repeat measurement), and 32 points were defined in area between 10 and 20 degrees. Then, each concentric circle area was equally divided into four sectors according to the ETDRS grid, with parafovea sector having 7 points and perifovea sector having 8 points. The average sensitivity (dB) in parafovea, perifovea, and each sector was computed (Fig. 1C: foveal center: 1 point at the center. Parafovea: 28 points in 10 degrees area, the area inside the smaller white circle.

Perifovea: 32 points in the area between 10 and 20 degrees, the ring between the two white circles). When calculating RS at each sector, we counted points on the left border line of ETDRS subfield but excluded those on the right border line for right eyes, and vice versa (Fig. 3).

Statistical Analysis

Statistical analysis was performed by Statistical Package for the Social Sciences (SPSS, IBM Corporation, Chicago, IL, USA) statistical software version 25.0. Categorical variables were expressed as number (%). Descriptive statistics with and without normal distribution were expressed as mean ± standard (SD) and median (P25, P75), respectively. Data were compared between groups by χ^2 test, Kruskall–Wallis test, or one-way analysis of variance (ANOVA) test, as appropriate. The change of BCVA, IRDs, and RS at each follow-up month was defined as subtracting the preoperative data from the postoperative data, marked with prefix "Δ." Repeated measures analysis of variance was used to evaluate differences in the chronologic data. The correlations between the change of IRDs and RS were evaluated using Spearman correlations. A multivariate linear regression model was performed to analyze the association
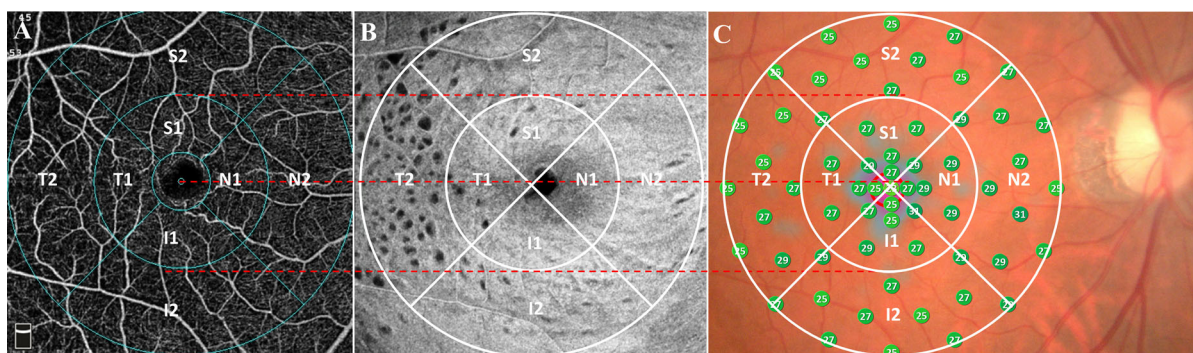

Fig. 1 The parafovea [inner superior (S1), inner inferior (I1), inner nasal (N1), and inner temporal (T1)] and perifovea [outer superior (S2), outer inferior (I2), outer nasal (N2), and outer temporal (T2)] of the ETDRS grid. **A** Superficial vessel density showed on the macular central 6×6 mm^2 area of en-face OCTA. **B** Inner retinal dimples appeared like a "darker spot" on en-face OCTA. **C** The distribution of 61 stimulus points covering 20 degrees on MP-3: foveal center, 1 point at the center; parafovea, 28 points in 10 degrees area (the area inside the smaller white circle); perifovea, 32 points in area between 10 and 20 degrees (the ring between the two white circles). *OCTA* optical coherence tomography angiography, *MP-3* microperimetry-3, *ETDRS* early treatment diabetic retinopathy study
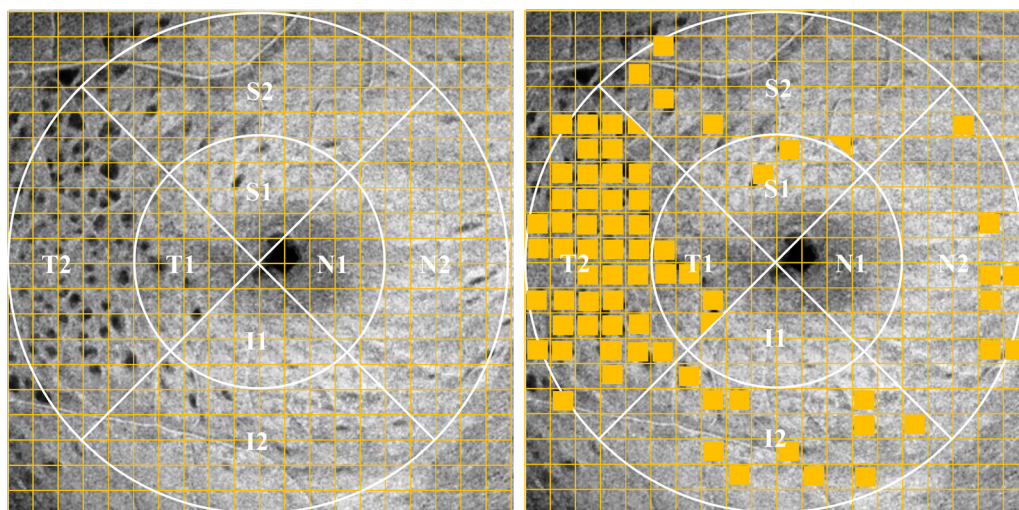
Fig. 2 Illustration of the quantitative method of analysis of IRDs. The 6×6 mm^2 area was divided into 20×20 squares of the same size. The number of the grids containing IRDs was counted manually in each ETDRS subfield. On the right image, the grids in yellow are IRDs that need to be counted. *ETDRS* early treatment diabetic retinopathy study, *IRDs* inner retina dimples; parafovea sector: inner superior (S1), inner inferior (I1), inner nasal (N1), and inner temporal (T1); perifovea sector: outer superior (S2), outer inferior (I2), outer nasal (N2), and outer temporal (T2)
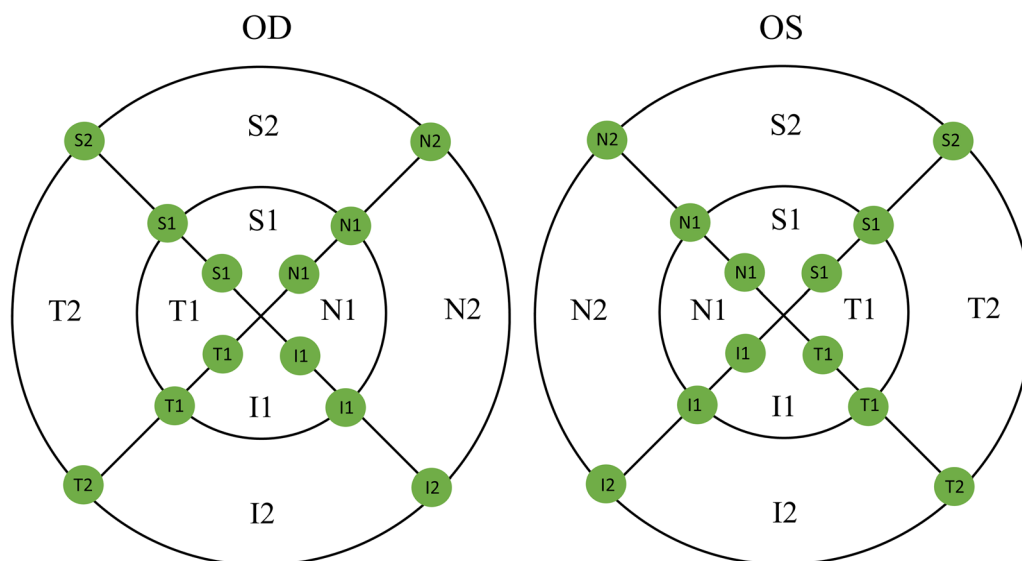

Fig. 3 The belonging area of the values on the cross line are illustrated. For the right eye, the points on the left border line of ETDRS subfield were counted, whereas the points on the right borderline were excluded. For left eye, the points on the right border line of ETDRS subfield were counted, whereas the points on the left borderline were excluded. The same assignment for points on borderlines were applied when calculating RS at each sector. *ETDRS* early treatment diabetic retinopathy study, *RS* retinal sensitivity. Parafovea sector: inner superior (S1), inner inferior (I1), inner nasal (N1), and inner temporal (T1). Perifovea sector: outer superior (S2), outer inferior (I2), outer nasal (N2), and outer temporal (T2). OD: the right eye; OS: the left eye
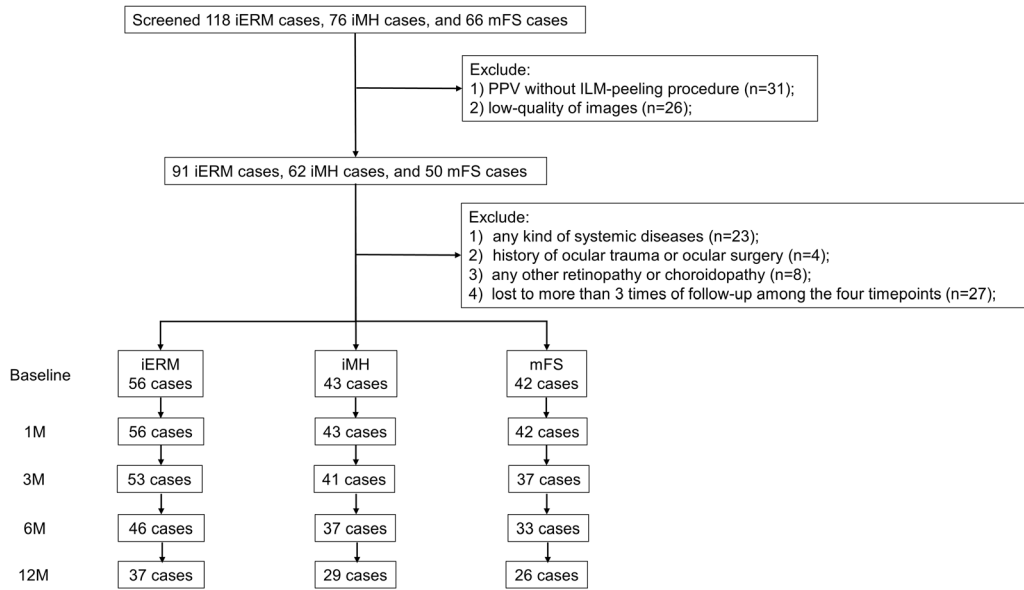
Fig. 4 Flow-chart of the study. *iERM* idiopathic epiretinal membrane, *iMH* idiopathic macular hole, *mFS* myopic foveoschisis, *ILM* internal limiting membrane, *PPV* pars plana vitrectomy, *1 M* 1-month follow-up, *3 M* 3-month follow-up, *6 M* 6-month follow-up, *12 M* 12-month follow-up

between baseline characteristics and the number of IRDs after adjusting for covariates with $p < 0.1$ in univariate analysis. A p value less than 0.05 was considered statistically significant.

RESULTS

Patient Demographic and Clinical Characteristics

As shown in Fig. 4, a total of 141 eyes from 141 patients were included in the current study, consisting of 43 iMH cases, 56 iERM cases, and 42 mFS cases. Reasons for the missing data in the follow-ups included: patients' routine follow-ups were competed at other hospitals, temporary traffic restrictions during the course of coronavirus disease 2019 (COVID-19) pandemic, patients suffered from other health issues, or patients were not contactable. The baseline characteristics are shown in Table1. There were significant differences in age ($p < 0.001$), axial length ($p < 0.001$) and preoperative BCVA ($p < 0.001$), tamponade

substance during surgery ($p = 0.003$), parafovea SVD ($p = 0.014$), parafovea RS ($p < 0.001$), and perifovea RS ($p < 0.001$) among three diseases.

The Progression and Distribution of IRDs

None of the patients had IRDs preoperatively. All patients (100%) had IRDs after surgery at ILM-peeled area. Postoperative OCT images showed the depth IRDs went through the ganglion cell layer (GCL) without reaching IPL (Fig. 5 A–C).

Figure 6 showed the number and distribution of IRDs in three diseases Table 2. The number of IRDs increased constantly within 6 months after surgery in all three diseases. Patients with iMH presented with the most IRDs across all the timepoints, whereas those with mFS presented with the least IRDs.

Figure 7A–C showed the distribution of IRDs in three diseases. In iMH, most IRDs were found in temporal sectors in both parafovea and perifovea (parafovea: $p = 0.008$ at 1 M, $p = 0.01$ at 3 M, $p = 0.004$ at 6 M, and $p = 0.006$ at 12 M; perifovea: $p < 0.001$ at 1 M, $p = 0.006$ at 3, $p = 0.015$ at 6 M, and $p = 0.01$ at 12 M) (Fig. 7A).

Table 1 Clinical characteristics of patients in three groups

Clinical characteristics	iMH (n = 43)	iERM (n = 56)	mFS (n = 42)	p value
Age (years)	60.6 ± 12.0	63.9 ± 10.3	54.1 ± 10.9	< 0.001
Sex female	35 (81.4)	44 (78.6)	33 (78.6)	0.930
Duration of symptom (months)	6 (2.4, 12)	12 (6, 36)	12 (3.6, 36)	0.002
Axial length (mm)	23.33 (22.69, 24.31)	23.34 (22.54, 23.91)	28.20 (26.76, 30.43)	< 0.001
Preoperative BCVA (logMAR)	0.80 (0.50, 1.00)	0.50 (0.30, 0.50)	0.70 (0.40, 1.00)	< 0.001
Phacoemulsification	40 (97.7)	52 (92.9)	39 (92.9)	0.114
Tamponade substance				0.003
Fluid, air exchange	38 (88.4)	55 (98.2)	32 (76.2)	–
C3F8	5 (11.6)	1 (1.8)	5 (11.9)	–
Silicone oil	0 (0.0)	0 (0.0)	5 (11.9)	–
SVD				
Parafovea SVD	51.1 (45.8, 54.0)	47.9 (44.7, 50.9)	47.8 (12.8, 52.7)	
Perifovea SVD	48.3 (44.9, 51.4)	50.1 (46.3, 52.9)	48.3 (39.8, 52.2)	0.014
RS (dB)				0.380
Parafovea RS	21.0 (19.2, 23.2)	22.6 (20.9, 24.3)	19.6 (16.2, 23.1)	
Perifovea RS	24.8 (21.7, 25.7)	22.5 (24.2, 19.6)	21.9 (16.3, 23.7)	< 0.001

BCVA best corrected visual acuity, *C3F8* perfluoropropane, *SVD* superficial vessel density, *RS* retina sensitivity, *iMH* idiopathic macular hole, *iERM* idiopathic epiretinal membrane, *mFS* myopic foveoschisis

In iERM, most IRDs were found in temporal sectors in both parafovea and perifovea (parafovea: $p < 0.001$ at 1 M, $p = 0.001$ at 3 M, $p = 0.042$ at 6 M, and $p = 0.003$ at 12 M; perifovea: $p < 0.001$ at 1 M, 3 M, 6 M, 12 M) (Fig. 7B). In mFS, most IRDs were found in T1 of parafovea across all the timepoints, although statistical significance was not reached. In perifovea, most IRDs were found in T2 ($p = 0.009$ at 1 M, $p < 0.001$ at 3 M) during follow-up (Fig. 7C).

Visual Function After Surgery

The mean BCVA and foveal macular RS improved after surgery in all patients (Fig. 8A, B; Table 3). In iMH and mFS, RS was only improved in parafovea but not perifovea. In iERM, however, no significant improvement of

RS was observed in parafovea or perifovea (Fig. 8C, D; Table 4).

In parafovea, the difference of ΔRS in each sector was not significant among all patients during follow-up. In perifovea, the difference of ΔRS in each sector was not significant in iERM or mFS. However, a significant difference in ΔRS among different sectors was observed in iMH, with T2 being most pronounced across all the timepoints ($p = 0.001$ at 1 M, $p = 0.001$ at 3 M, $p = 0.011$ at 6 M, $p = 0.007$ at 12 M) (Fig. 9).

Association Between the Change Value of IRDs and RS

As shown in Table 5, in iMH, the number of IRDs was negatively associated with the change of RS in perifovea at 1 M, 3 M, 6 M, and 12 M. In iERM, the number of IRDs was negatively correlated with the change of RS in parafovea and
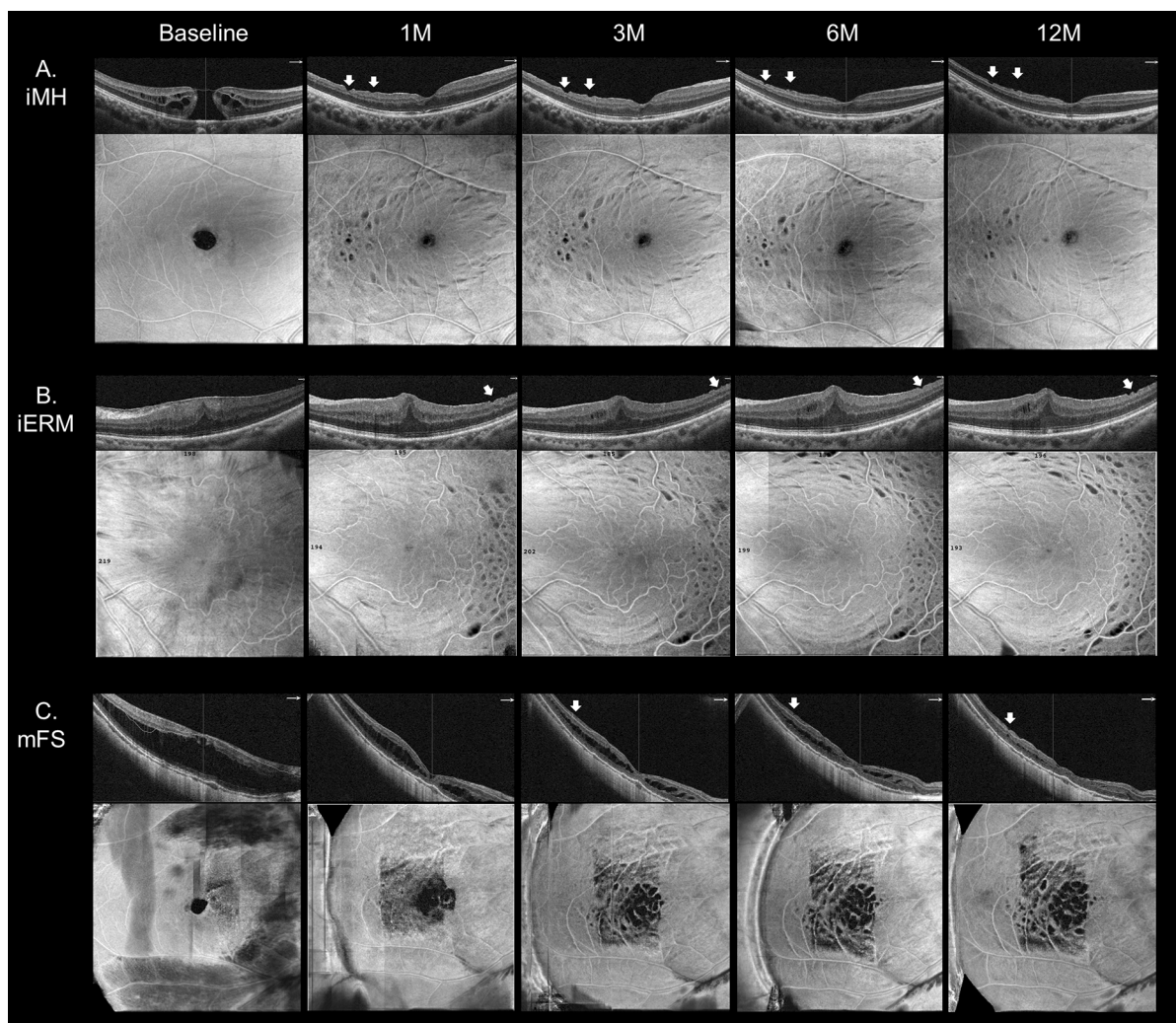
Fig. 5 Pre- and postoperative months 1, 3, 6, and 12 (1 M, 3 M, 6 M, 12 M) optical coherence tomography (OCT) images. The depths of inner retinal dimples (IRDs) were shown plainly on cross-sectional images at macular foveal pit (arrows). The distribution of IRDs was showed on en-face OCT images. **A** Images of a 62-year-old woman with idiopathic macular hole (iMH). **B** Images of a 65-year-old man with idiopathic epiretinal membrane (iERM). **C** Images of a 47-year-old woman with myopic foveoschisis (*mFS*)

perifovea at 3 M, 6 M, and 12 M. In mFS, however, no significant relationship could be established between the IRDs and RS at parafovea or perifovea postoperatively.

Baseline Characteristics Related to IRDs

To figure out risk factors associated for early and late stage of IRDs improvement, we analyzed the association between baseline characteristics and IRDs at 1 M and 12 M. As shown in Table 6,

univariate analysis showed that axial length and SVD at baseline were significantly associated with IRDs at 1 M and 12 M. After adjusting for potential confounders, multivariable linear regression model showed that that baseline axial length was significantly associated with IRDs at both 1 M and 12 M (1 M: $\beta = -0.226$, $p = 0.026$; 12 M: $\beta = -0.284$, $p = 0.038$) (Table 7).
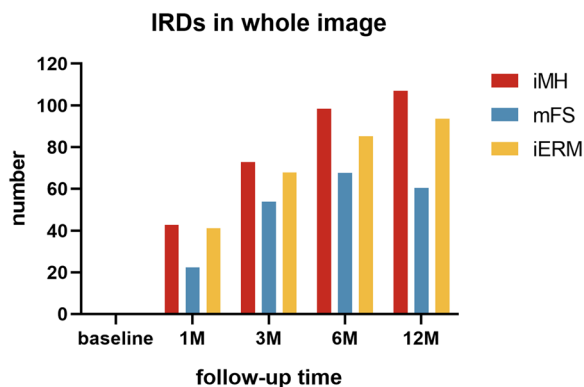
Fig. 6 The total number of inner retinal dimples in three diseases at each timepoint. *iMH* idiopathic macular hole, *iERM* idiopathic epiretinal membrane, *mFS* myopic foveoschisis, *IRDs* inner retinal dimples

Table 2 The total number of IRDs in three diseases at each timepoint

	iMH	**iERM**	**mFS**	*p* **value**
1 M	31 (12, 72)	38 (19, 57)	17 (7, 34)	0.007
3 M	66 (46, 101)	57 (29, 100)	49 (28, 73)	0.209
6 M	82 (59, 128)	76 (53, 116)	62 (34, 93)	0.065
12 M	92 (62, 148)	97 (62, 124)	49 (25, 77)	0.003

IRDs inner retinal dimples, *iMH* idiopathic macular hole, *iERM* idiopathic epiretinal membrane, *mFS* myopic foveoschisis

DISCUSSION

In the present study, we found that IRDs increased gradually at ILM-peeled area with time in iMH, iERM, and mFS. Most IRDs distributed in temporal sector in both perifovea and parafovea, interrupting the ganglion cell layer. The progress of IRDs may influence postoperative RS only in iMH and iERM. Then we identified that baseline axial length was a protective factor for IRDs after ILM peeling.

Our results showed that IRDs occurred at superficial layer of inner retina at 1 M and gradually went through GCL. ILM is composed of vitreous-facing endfoot membranes of Müller cells and basal lamina [16]. Histopathological studies [17, 18] showed that cellular fragments belonging to Müller cells appeared on the retinal side of peeled ILM. In vitro, Taylor et al. [19] emphasized the importance of physical support by ILM in maintaining the structure of inner retina. In vivo, the endfoot of Müller cells contain enormous mechanosensitive ion channels [20] and the processes of Müller cells penetrate nearly whole layers of retina as "bridges" with photoreceptor's axons [21]. Once biomechanical changes were detected, mechanosensitive channels may transfer certain signals to the entire retina. The loss of inner retina mechanic support might influence the layer near RNFL initially and then expand along the processes of Müller cells to the entire retina layers. Thus, we suspected that the lack of support in inner retina, stimulation of stretch force, and damage to the endfoot of Müller cells might contribute to the formation of IRDs. Nevertheless, we found that IRDs did not reach IPL, which might be because the supracellular alignment of tissue redistributes mechanical energy before it reaches the nucleus [22]. Previous electron microscopic findings showed [23] that the perikaryons of Müller cells are located in the inner nuclear layer. To note, the follow-up period of our study is 12 months. Future study with prolonged follow-up is needed to investigate whether IRDs would expand along the processes of Müller cells in the long run.

Most IRDs were found in temporal sector in both perifovea and parafovea in our study, which might be explained by the following reasons. First, histological studies showed that the Henle fiber layer (HFL), which was composed of the processes of Müller cells, horizontally extends the most in the temporal retina and least in nasal retina [16], making the processes of Müller cells more prone to contraction and degeneration. Besides, Veronese et al. [24] found that the nasal side of the fovea was more resistant to traction because nerve fibers and retinal ganglion cells (RGCs) were bound together closely in the papilla–macular bundle, which may make it difficult for dimples at the nasal subfield to "sink" widely. In addition, the retina thinning was mostly seen in the temporal subfield after ILM peeling [25–27], because of foveal displacement toward optic disc. The thinner retina in temporal field might make it
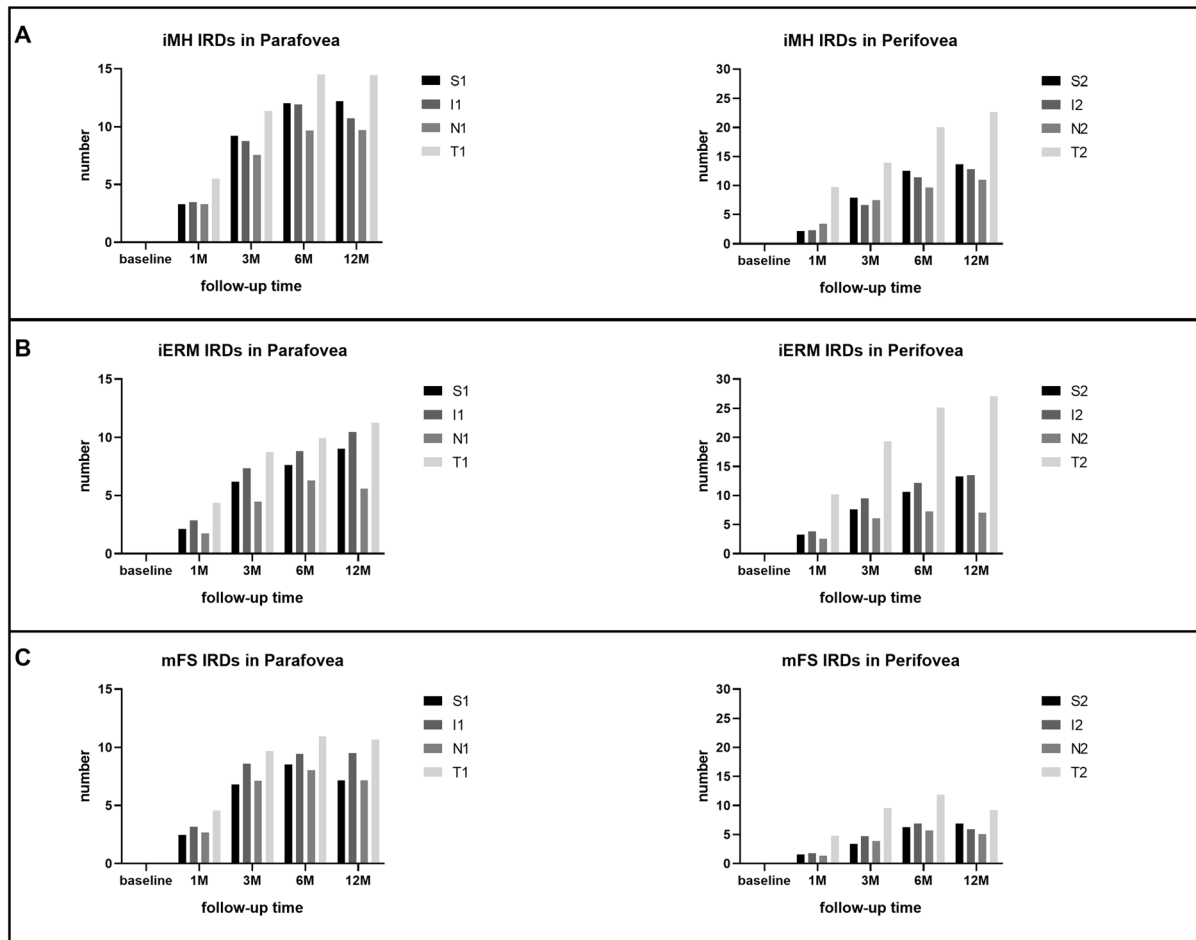
Fig. 7 The number of inner retinal dimples (*IRDs*) at different sectors in three diseases. Parafovea sector: inner superior (S1), inner inferior (I1), inner nasal (N1), and inner temporal (T1). Perifovea sector: outer superior (S2), outer inferior (I2), outer nasal (N2), and outer temporal (T2). **A** The distribution of IRDs at different sectors in iMH. **B** The distribution of IRDs at different sectors in iERM. **C** The distribution of IRDs at different sectors in mFS. *iMH* idiopathic macular hole, *iERM* idiopathic epiretinal membrane, *mFS* myopic foveoschisis

more prone to contracting damage, thus forming more IRDs.

Next, we investigated the change of visual function after ILM peeling. Great improvement in BCVA was observed in all patients. However, RS was improved only in parafovea of iMH and mFS. No improvement in RS was observed in the perifovea, particularly in the temporal sector of iMH (RS actually declined with time after ILM peeling; Fig. 9). Ultrastructure research [16, 28] showed that Müller cells in HFL supported structural stability through increasing compliance and resistance by its "z-shape" at the parafovea. In contrast, at the perifovea,

shorter Müller cells aligned in a vertical pattern as pillars, through which it was easier to transmit mechanical stress directly to photoreceptors without a "z-shaped" "spring buffer." Furthermore, the densities of photoreceptor and RGCs were less in the temporal sector compared with the nasal retina [29], resulting in the insufficient compensation of light path in this area.

This study illustrated a negative correlation between IRDs and RS beyond central fovea in iMH or iERM, which might explain why some patients experienced scotoma and metamorphopsia after ILM peeling. IRDs were possibly secondary to damage in Müller cells. Being
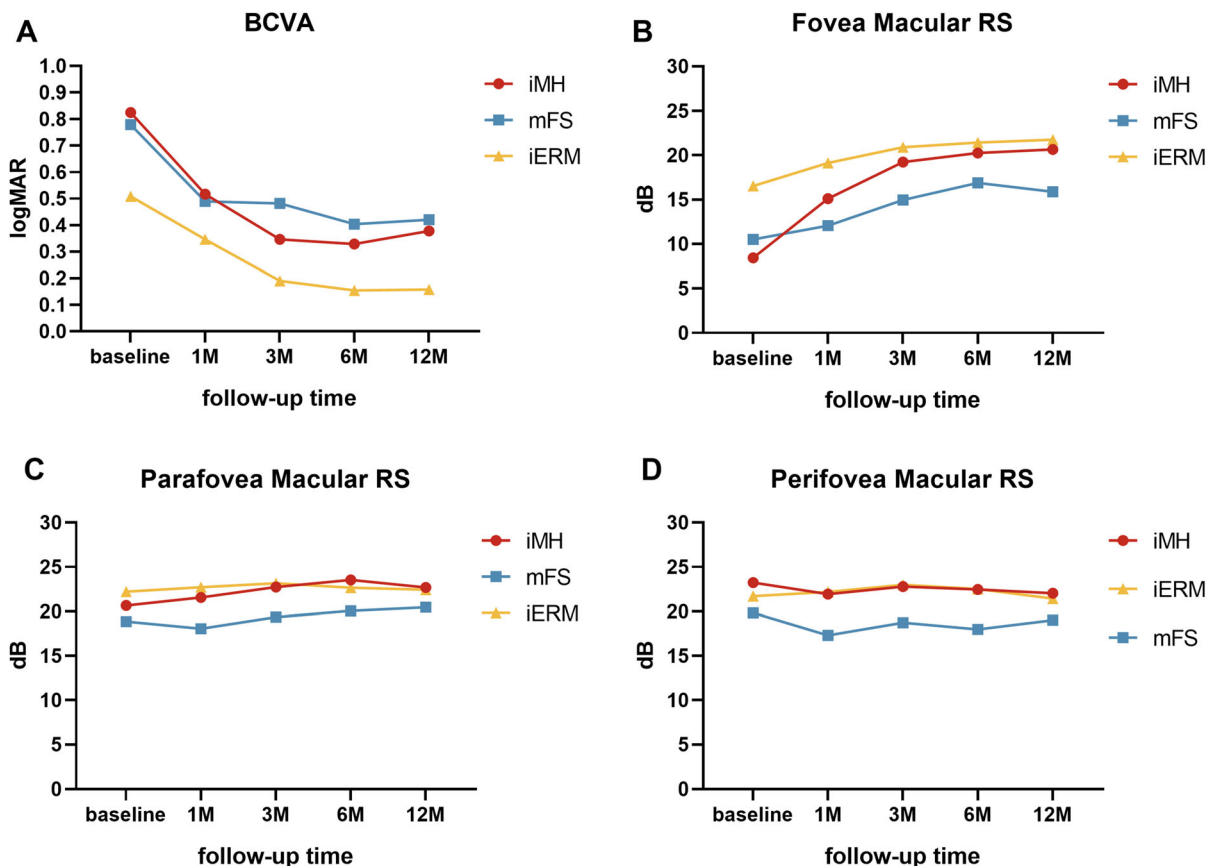
Fig. 8 Vision function in all patients. **A** The progress of mean BCVA in three diseases. **B** The progress of fovea macular RS in three diseases. **C** The progress of parafovea macular RS in three diseases. **D** The progress of perifovea macular RS in three diseases. *BCVA* best corrected visual acuity, *RS* retinal sensitivity, *iMH* idiopathic macular hole, *iERM* idiopathic epiretinal membrane, *mFS* myopic foveoschisis

Table 3 BCVA at each timepoint in three diseases

	iMH	iERM	mFS	*p* value
Baseline	0.80 (0.50, 1.00)	0.50 (0.30, 0.50)	0.70 (0.40, 1.00)	< 0.001
1 M	0.50 (0.30, 0.70)	0.30 (0.20, 0.40)	0.40 (0.30, 0.70)	0.002
3 M	0.30 (0.20, 0.50)	0.15 (0.10, 0.30)	0.40 (0.20, 0.70)	< 0.001
6 M	0.30 (0.20, 0.40)	0.10 (0.00, 0.20)	0.35 (0.15, 0.70)	< 0.001
12 M	0.30 (0.20, 0.50)	0.10 (0.00, 0.20)	0.40 (0.15, 0.70)	< 0.001

BCVA best corrected visual acuity, *iMH* idiopathic macular hole, *iERM* idiopathic epiretinal membrane, *mFS* myopic foveoschisis

Table 4 RS at each each timepoint in three diseases

	Baseline	1 M	3 M	6 M	12 M	p^a value
Fovea						
iMH	7.0 (0.0, 15.0)	15.0 (11.0, 19.0)	21.0 (17.0, 23.0)	21.0 (17.0,25.0)	21.0 (15.0, 24.0)	< 0.001
iERM	17.0 (14.0, 19.5)	19.0 (17.0, 22.3)	21.0 (19.0, 23.0)	23.0 (19.0, 23.0)	23.0 (19.0, 24.0)	0.046
mFS	11.0 (2.3, 17.0)	13.0 (7.0, 17.0)	15.0 (11.0, 19.0)	17.0 (13.0, 23.0)	17.0 (7.0, 25.0)	0.029
Parafovea						
iMH	21.0 (19.2, 23.2)	21.6 (19.4, 23.7)	23.8 (21.6, 24.9)	23.8 (21.5, 25.8)	23.0 (20.1, 25.6)	< 0.001
iERM	22.6 (20.9, 24.3)	23.2 (21.6, 24.5)	23.8 (21.9, 24.8)	23.2 (21.5, 24.4)	23.4 (20.9, 24.9)	0.874
mFS	19.6 (16.2, 23.1)	17.4 (14.5, 22.5)	19.9 (15.9, 22.6)	20.6 (16.5, 24.3)	20.4 (16.6, 25.2)	0.023
Periovea						
iMH	24.8 (21.7, 25.7)	22.1 (20.5, 24.5)	23.6 (21.9, 25.2)	23.9 (21.2, 24.7)	23.5 (19.5, 24.4)	< 0.001
iERM	22.5 (24.2, 19.6)	23.0 (21.6, 24.7)	23.9 (21.3, 25.7)	23.9 (20.5, 24.6)	22.4 (18.2, 24.7)	0.738
mFS	21.9 (16.3, 23.7)	16.6 (13.0, 22.8)	19.5 (13.5, 23.6)	19.6 (12.3, 23.7)	19.9 (15.3, 22.9)	0.306

RS retinal sensitivity, *iMH* idiopathic macular hole, *iERM* idiopathic epiretinal membrane, *mFS* myopic foveoschisis
[a]Analysis of variance for repeated measurements

interposed by neurons and photoreceptors, Müller cells participate in light transmitting through endfeet to main process as "optical fiber" and lend support to surrounding microenvironment functionally and metabolically [16, 21, 30]. ILM peeling might damage the endfoot of Müller cells, hampering the microenvironment of RGCs, causing anoikis and eventually leading to the loss of visual function [31–33]. To support this, Akino et al. [34] confirmed that visual field defects were associated with GCL thinning in iMH after ILM peeling. However, no significant correlation between IRDs and RS was found in mFS, which might be due to the low IRDs count after ILM peeling.

We also explored the relationship between preoperative factors and IRDs, finding a significant negative correlation between axial length and IRDs at 1 M and 12 M. Also, patients with mFS presented the least IRDs across all the timepoints, which lent further support of the effect of axial length on postoperative IRDs. Long-term elongated axial length would enhance Müller cell gliosis [35]. The overstretch of Müller cell processes along with HFL may
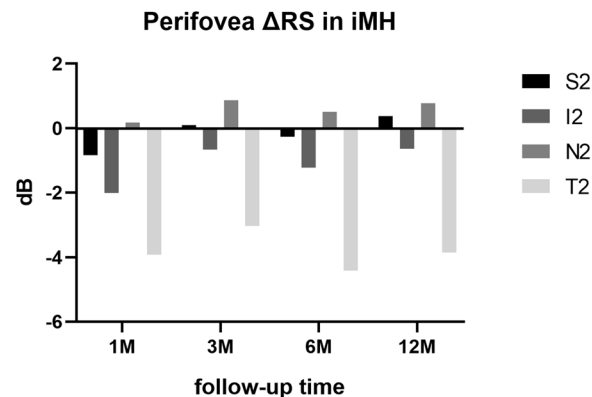

Fig. 9 ΔRS among different sectors in idiopathic macular hole. Perifovea sector: outer superior (S2), outer inferior (I2), outer nasal (N2), and outer temporal (T2). *RS* retinal sensitivity, *iMH* idiopathic macular hole

compromise the capacity of photoreceptors synapses [28]. Hence, we hypothesized that the retina in mFS might have already adapted to low metabolic demands under abnormal Müller cells, downregulating the mechanical influence caused by tearing the glial endfoot of Müller cells.

Table 5 Association between the change value of IRDs and RS

ΔRS	ΔIRDs of iMH		ΔIRDs of iERM		ΔIRDs of mFS	
	Parafovea	Perifovea	Parafovea	Perifovea	Parafovea	Perifovea
1 M	$r = -0.088$, $p = 0.288$	$r = -0.026$, $p = 0.120$	$r = 0.062$, $p = 0.448$	$r = -0.106$, $p = 0.235$	$r = 0.158$, $p = 0.090$	$r = -0.048$, $p = 0.609$
3 M	$r = -0.267$, $p = 0.001$	$r = -0.166$, $p = 0.039$	$r = -0.257$, $p = 0.003$	$r = -0.251$, $p = 0.004$	$r = -0.126$, $p = 0.210$	$r = -0.172$, $p = 0.087$
6 M	$r = -0.021$, $p = 0.838$	$r = -0.298$, $p = 0.002$	$r = -0.221$, $p = 0.030$	$r = -0.302$, $p = 0.019$	$r = -0.107$, $p = 0.301$	$r = -0.060$, $p = 0.563$
12 M	$r = -0.208$, $p = 0.042$	$r = -0.306$, $p = 0.002$	$r = -0.301$, $p = 0.047$	$r = -0.324$, $p = 0.025$	$r = -0.058$, $p = 0.636$	$r = -0.095$, $p = 0.442$

IRDs inner retinal dimples, *RS* retinal sensitivity, *iMH* idiopathic macular hole, *iERM* idiopathic epiretinal membrane, *mFS* myopic foveoschisis

Table 6 Univariate analysis of demographic, clinical, and morphological baseline data with postoperative IRDs

	1 M		12 M	
Age	$r = 0.111$	$p = 0.217$	$r = -0.002$	$p = 0.987$
Sex		$p = 0.668$		$p = 0.176$
Male	36 (9, 54)	–	109 (57, 133)	–
Female	24 (12, 53)	–	71 (44, 109),	–
Duration of symptom	$r = -1.121$	$p = 0.176$	$r = -0.073$	$p = 0.528$
Axial length	$r = -0.272$	$p = 0.002$	$r = -0.316$	$p = 0.005$
Tamponade substance		$p = 0.068$		$p = 0.432$
Fluid, air exchange	30 (12, 55)	–	75 (47, 121)	–
C3F8	28 (8, 39)	–	79 (13, 88)	–
Silicone oil	9 (2,17)	–	51 (27, 89)	–
SVD	$r = 0.183$	$p = 0.046$	$r = 0.130$	$p = 0.257$

IRDs inner retinal dimples, *C3F8* Perfluoropropane, *SVD* superficial vessel density

To our knowledge, this is the first study to quantitatively compare inner retina defect after ILM peeling combined with PPV among iMH, iERM, and MFS. Based on the findings of our study, we consider that ophthalmologist may be more conservative in the temporal sector during ILM peeling, especially in patients with normal axial length and adherent ILM–ERM. Future studies may pay attention to the biomechanical importance of ILM and extracellular matrix components of the inner retina to gain further insights into the pathogenesis of IRDs after ILM peeling.

Our study has several limitations, the first being that is a single-center retrospective study with relatively small sample size. Multicenter studies with larger sample sizes are warranted in the future. Second, all the procedures were

Table 7 Linear regression analysis for variables related to postoperative IRDs

	1 M			12 M		
	β	95% CI	p value	β	95% CI	p value
Axial length	−0.251	−5.036, − 0.699	0.010	−0.293	−9.746, −0.837	0.020
SVD	0.278	−0.787, 1.343	0.607	−0.067	−1.261, 2.200	0.591

IRDs inner retinal dimples, *SVD* superficial vessel density, *CI* confidence interval

completed by the same surgeon in our study, which limits the generalizability of our results. However, this assured the homogeneity of procedures. Additionally, it is reported that ICG may have adverse effects on retina. Therefore, we cannot be sure that the formation of IRDs is purely the result of mechanical stretch, since the dye only stays within eyes for less than 30 s. Future studies need to investigate IRDs after ILM peeling using a dye other than ICG.

CONCLUSIONS

Our study suggests that ophthalmologists may avoid the temporal sector of parafovea and perifovea, especially in eyes with normal axial length or strong ILM–ERM adherence during ILM peeling.

Declarations

REFERENCES

1. Chatziralli IP, Theodossiadis PG, Steel DHW. Internal limiting membrane peeling in macular hole surgery; why, when, and how? Retina. 2018;38(5):870–82.

2. Modi A, Giridhar A, Gopalakrishnan M. Spectral domain optical coherence tomography-based microstructural analysis of retinal architecture post internal limiting membrane peeling for surgery of idiopathic macular hole repair. Retina. 2017;37(2):291–8.

3. Terasaki H, Miyake Y, Nomura R, et al. Focal macular ERGs in eyes after removal of macular ILM during macular hole surgery. Invest Ophthalmol Vis Sci. 2001;42(1):229–34.

4. Tadayoni R, Paques M, Massin P, Mouki-Benani S, Mikol J, Gaudric A. Dissociated optic nerve fiber layer appearance of the fundus after idiopathic epiretinal membrane removal. Ophthalmology. 2001;108(12):2279–83.

5. Arias L, Padrón-Pérez N, Flores-Moreno I, et al. Internal limiting membrane peeling versus non-peeling to prevent epiretinal membrane development in primary rhegmatogenous retinal detachment: a swept-source optical coherence tomography study with a new postoperative classification system. Retina. 2020;40(7):1286–98.

6. Navajas EV, Schuck N, Govetto A, et al. En face optical coherence tomography and optical coherence tomography angiography of inner retinal dimples after internal limiting membrane peeling for full-thickness macular holes. Retina. 2020;40(3):557–66.

7. Tao J, Yang J, Wu Y, et al. Internal limiting membrane peeling distorts the retinal layers and induces scotoma formation in the perifoveal temporal macula. Retina. 2022;42(12):2276–83.

8. Tadayoni R, Svorenova I, Erginay A, Gaudric A, Massin P. Decreased retinal sensitivity after internal limiting membrane peeling for macular hole surgery. Br J Ophthalmol. 2012;96(12):1513–6.

9. Chae JB, Choi DK, Kim JG. Nerve fiber layer irregularity after internal limiting membrane peeling, seen by spectral domain optical coherence tomography. Eye (Lond). 2011;25(11):1515–6.

10. Nukada K, Hangai M, Ooto S, Yoshikawa M, Yoshimura N. Tomographic features of macula after successful macular hole surgery. Invest Ophthalmol Vis Sci. 2013;54(4):2417–28.

11. Mitamura Y, Ohtsuka K. Relationship of dissociated optic nerve fiber layer appearance to internal limiting membrane peeling. Ophthalmology. 2005;112(10):1766–70.

12. Ito Y, Terasaki H, Takahashi A, Yamakoshi T, Kondo M, Nakamura M. Dissociated optic nerve fiber layer appearance after internal limiting membrane peeling for idiopathic macular holes. Ophthalmology. 2005;112(8):1415–20.

13. Sakimoto S, Ikuno Y, Fujimoto S, Sakaguchi H, Nishida K. Characteristics of the retinal surface after internal limiting membrane peeling in highly myopic eyes. Am J Ophthalmol. 2014;158(4):762-8.e1.

14. Steel DH, Dinah C, White K, Avery PJ. The relationship between a dissociated optic nerve fibre layer appearance after macular hole surgery and Muller cell debris on peeled internal limiting membrane. Acta Ophthalmol. 2017;95(2):153–7.

15. Mokrane A, Zureik A, Bonnin S, et al. Retinal sensitivity correlates with the superficial vessel density and inner layer thickness in diabetic retinopathy. Invest Ophthalmol Vis Sci. 2021;62(14):28.

16. Reichenbach A, Bringmann A. Glia of the human retina. Glia. 2020;68(4):768–96.

17. Beyazyildiz Ö, Tirhiş MH, Hekimoğlu ER, et al. Histopathological analysis of internal limiting membrane surgically peeled from eyes with epiretinal membrane. Curr Eye Res. 2016;41(2):258–65.

18. Bando H, Ikuno Y, Choi JS, Tano Y, Yamanaka I, Ishibashi T. Ultrastructure of internal limiting membrane in myopic foveoschisis. Am J Ophthalmol. 2005;139(1):197–9.

19. Taylor L, Arnér K, Taylor IH, Ghosh F. Feet on the ground: physical support of the inner retina is a strong determinant for cell survival and structural preservation in vitro. Invest Ophthalmol Vis Sci. 2014;55(4):2200–13.

20. Vecino E, Rodriguez FD, Ruzafa N, Pereiro X, Sharma SC. Glia-neuron interactions in the mammalian retina. Prog Retin Eye Res. 2016;51:1–40.

21. Bringmann A, Syrbe S, Görner K, et al. The primate fovea: structure, function and development. Prog Retin Eye Res. 2018;66:49–84.

22. Nava MM, Miroshnikova YA, Biggs LC, et al. Heterochromatin-driven nuclear softening protects the genome against mechanical stress-induced damage. Cell. 2020;181(4):800-17.e22.

23. Wolf S, Schnurbusch U, Wiedemann P, Grosche J, Reichenbach A, Wolburg H. Peeling of the basal membrane in the human retina: ultrastructural effects. Ophthalmology. 2004;111(2):238–43.

24. Pichi F, Lembo A, Morara M, et al. Early and late inner retinal changes after inner limiting membrane peeling. Int Ophthalmol. 2014;34(2):437–46.

25. Loiudice P, Pellegrini M, Montesel A, et al. Negative correlation between retinal displacement and ganglion cell layer thickness changes in eyes with epiretinal membrane. Eur J Ophthalmol. 2020;30(6):1424–31.

26. Faria MY, Ferreira NP, Mano S, Cristóvao DM, Sousa DC, Monteiro-Grillo ME. Internal retinal layer thickness and macular migration after internal limiting membrane peeling in macular hole surgery. Eur J Ophthalmol. 2018;28(3):311–6.

27. Chou HD, Chong YJ, Teh WM, et al. Nasal or temporal internal limiting membrane flap assisted by sub-perfluorocarbon viscoelastic injection for macular hole repair. Am J Ophthalmol. 2021;223: 296–305.

28. Govetto A, Hubschman JP, Sarraf D, et al. The role of Müller cells in tractional macular disorders: an optical coherence tomography study and physical model of mechanical force transmission. Br J Ophthalmol. 2020;104(4):466–72.

29. Finlay BL, Franco EC, Yamada ES, et al. Number and topography of cones, rods and optic nerve axons in new and old world primates. Vis Neurosci. 2008;25(3):289–99.

30. Toft-Kehler AK, Skytt DM, Kolko M. A Perspective on the müller cell-neuron metabolic partnership in the inner retina. Mol Neurobiol. 2018;55(6): 5353–61.

31. Ikeda T, Nakamura K, Sato T, Kida T, Oku H. Involvement of anoikis in dissociated optic nerve fiber layer appearance. Int J Mol Sci. 2021;22(4): 1724.

32. Sabry D, El-Kannishy A, Kamel R, Abou SW. Correlation between En face optical coherence tomography defects of the inner retinal layers and ganglion cell inner plexiform layer analysis after internal limiting membrane peeling for idiopathic full-thickness macular hole. Invest Ophthalmol Vis Sci. 2016;57(9):444–50.

33. Dysli M, Ebneter A, Menke MN, et al. Patients with epiretinal membranes display retrograde maculopathy after surgical peeling of the internal limiting membrane. Retina. 2019;39(11):2132–40.

34. Akino K, Nagai N, Watanabe K, et al. Risk of newly developing visual field defect and neurodegeneration after pars plana vitrectomy for idiopathic epiretinal membrane. Br J Ophthalmol. 2021;105(12):1683–7.

35. Vogt D, Stefanov S, Guenther SR, et al. Comparison of vitreomacular interface changes in myopic foveoschisis and idiopathic epiretinal membrane foveoschisis. Am J Ophthalmol. 2020;217:152–61.